Fluid Phase Equilibria 382 (2014) 10–20

Contents lists available at ScienceDirect

Fluid Phase Equilibria

journal homepage: www.elsevier.com/locate/fluid

# Effect of water on methane and carbon dioxide sorption in clay minerals by Monte Carlo simulations

Zhehui Jin[a], Abbas Firoozabadi[a,b,*]

[a] Reservoir Engineering Research Institute, Palo Alto, CA, USA
[b] Yale University, New Haven, CT, USA

ARTICLE INFO

*Article history:*
Received 4 April 2014
Received in revised form 23 July 2014
Accepted 24 July 2014
Available online 2 August 2014

*Keywords:*
Sorption in clay
Shale media
Nanopores

ABSTRACT

Shale is mainly composed of: (1) inorganic, and (2) organic materials. As an important constituent of inorganic matter, clay minerals may affect gas-in-place of shale permeable media. Clay minerals are hydrophilic. Hydrophilicity may affect pore space saturation with water in shale media. In this work, we investigate the effect of water on methane and $CO_2$ sorption in clay minerals by using grand canonical Monte Carlo simulations. Our investigation reveals that water may significantly reduce methane and $CO_2$ sorption in clay nanopores. In small pores (1 nm), water and $CO_2$, and water and methane adsorbed in the same layer. In large pores (>2 nm), water molecules adsorb on the first layer, and $CO_2$ and methane form a weak second layer adsorption. $CO_2$ unlike methane both in pure and low water content conditions may form multi-layer adsorption at high pressure. Multilayer adsorption results in significant increase of sorption with pressure. Langmuir adsorption model cannot be used for such descriptions. Our study on sorption of $CO_2$ and water mixtures in clay minerals shows that with a small amount of water in the domain outside the nanopores, $CO_2$ sorption is significantly reduced. In larger pores (>2 nm), gas molecules mainly accumulate in the middle of the pores.



## 1. Introduction

Shale is composed of two distinct materials: organic and inorganic. The organic materials are mainly composed of kerogen, which is a mixture of organic chemical compounds. Organic matter in shale increases porosity [1] and the porosity of kerogen can be as high as 50% of the total porosity [2]. A study [3] suggests that gas sorption and dissolution in organic materials may significantly contribute to gas-in-place in shale gas reservoirs. In some organic-rich shale reservoirs, there is a strong correlation between methane sorption to the total organic content (TOC) [3–5]. Thermally mature kerogen may have larger micropore volume than that of immature kerogen resulting in higher ratio of gas sorption capacity [1].

In addition to organic matter, clay minerals may provide additional sorption capacity due to high internal surface area [6]. A few studies have reported that the clay mineral composition and its microporous structure may increase gas sorption capacity of organic-rich shales [7–9]. There are indications that clay minerals affect sorption in clay-rich shales [3,7,10–13]; clay minerals have micropore-to-mesopore structures which provide additional surface areas for gas sorption depending on the pore structures and clay chemical compositions [3]. Experimental and computational works [7,14] have shown that gas sorption in clay minerals can be comparable to shale rocks. Clays are generally made of large particles formed by stacks of sheets [15]. They are hydrophilic and moisture may occupy the surface sites.

Some shale gas reservoirs are water-saturated [16]. Preloaded water in clay-rich shales significantly reduces gas sorption [3] and even in the organic-rich shales, gas sorption capacity can be greatly reduced because of the moisture [17]. While kerogen is generally hydrophobic, clay minerals are hydrophilic; water can be easily adsorbed onto clay mineral surfaces reducing the total gas sorption capacity of shale. Experimental work [7] in clay minerals show that sorption capacity under moisture-equilibrated condition is substantially lower than that under the dry conditions. There are extensive experimental and computational works [18–28] on the effect of water on gas sorption in porous media, such as coals. The methane sorption capacity of moisture-equilibrated coals is substantially lower than the dry samples [20,29]. The adsorption of water is related to the hydrophilic sites from the oxygen-containing functional groups with a reduction of the available pore volume for gas sorption [27]. There are very limited studies on the effect of moisture on gas sorption in clay minerals and the underlying

* Corresponding author. Tel.: +1 650 326 9259.
*E-mail address:* af@rerinst.org (A. Firoozabadi).

http://dx.doi.org/10.1016/j.fluid.2014.07.035
0378-3812/

mechanisms. In contrast to coals, water association with clay surfaces is even stronger due to various partial/full charges of surface atoms. Additionally, some clay minerals, such as montmorillonite clay, have an cation-exchange ability to further enhance the hydrophilicity [30].

Molecular simulations [14,31,32] have been conducted in relation to gas sorption in dry clay minerals. In a recent work, we have applied grand canonical Monte Carlo (GCMC) simulations to investigate methane and $CO_2$ sorption in clay nanopores [14]. Due to the chemical heterogeneity, the structural and thermodynamic properties in clays are significantly different from that in conventional carbonaceous materials [14]. Coasne et al. [18] used the GCMC simulations to study the effect of water on sorption of methane and carbon dioxide in the slit-pore like nanoporous carbons. They preloaded water in carbon nanopores; the amount of water stayed constant in the process of gas sorption due to the high free energy barrier to desorb preadsorbed water and found that water greatly reduces gas sorption capacity, especially for methane. Coasne et al. [19] also investigated the effect of water on methane and carbon dioxide sorption in disordered porous carbons and observed a higher decrease in the sorption of methane than carbon dioxide. In both studies, the authors explained higher reduction of methane adsorption because of stronger interaction of $CO_2$–$H_2O$ than methane–$H_2O$ interaction. Very recently, Zhang et al. [33] used computer simulations to study methane sorption in dry and moist coals. They reported that methane sorption capacity decreases as moisture content increases. In contrast to carbonaceous materials, computational studies on the effect of water on gas sorption in clay minerals are limited. Botan et al. [34] used Monte Carlo and molecular dynamics simulations to study the structural and thermodynamic properties of carbon dioxide in hydrated sodium montmorillonite. The effect of water was not included in their work. To best of our knowledge, no computational and theoretical investigations have been made on the effect of water on gas sorption in clay minerals.

In this work, we use GCMC simulations to investigate the effect of water on methane and $CO_2$ sorption in clay-like slit pores. Methane is the main constituent of natural gases. Carbon dioxide is often present in the subsurface. Similar to gas sorption modeling in carbonaceous materials, we assume that the inter-pore interactions are negligible and gas adsorbs in nanometer slit-like pores. The solid surface in our work has a structure and charge of the montmorillonite clay consisting of two tetrahedral sheets fused to an octahedral sheet [35]. Montmorillonite clay has a large internal surface area, and shows a strong cation-exchange capacity [7]. It is one of major constituents of clay minerals in shale [3]. Montmorillonite clay consists of negatively charged silicate layers with Si atoms replaced by Al atoms in the tetrahedral sheet and Al atoms replaced by Mg atoms in the octahedral sheet [30]. The negative charges are compensated by interlayer counterions [36]. We use a full atomistic pore structure by duplicating the unit cell of montmorillonite clay proposed by Skipper et al. [37] and sodium ions as the interlayer counterions. By incorporating these features, we believe that our GCMC can provide fundamental understandings of the effect of water on gas sorption in clay minerals. This work is continuation of our previous work on gas sorption in dry clay minerals [14]. By combining these two works, we believe insight is provided into the fundamental understanding of gas sorption in clay and the effect of water (or moisture).

The remainder of this paper is organized as follows. In Section 2, we introduce the molecular simulation methods and define the molecular models we use. In Section 3, we investigate the effect of water on methane and $CO_2$ sorption in clay-like slit pores of various sizes and bulk densities of the gas molecules, as well as the preloaded water in the pores. We also study $CO_2$-$H_2O$ mixture sorption in clay nanopores of different sizes. In Section 4, we summarize the key conclusions and discuss implications.

**Table 1**
Atomic positions and effective charges in the unit cell.

| Atom | $x$ (nm) | $y$ (nm) | $z$ (nm) | $q$ (e) |
|---|---|---|---|---|
| O | 0.264 | 0.0 | 0.328 | −0.8 |
| O | 0.132 | 0.228 | 0.328 | −0.8 |
| O | 0.396 | 0.228 | 0.328 | −0.8 |
| O(OH) | 0.0 | 0.0 | 0.106 | −1.7175 |
| H(OH) | 0.08815 | 0.0 | 0.1434 | 0.7175 |
| Si | 0.264 | 0.152 | 0.273 | 1.2 |
| Si | 0.0 | 0.305 | 0.273 | 1.2 |
| O | 0.264 | 0.152 | 0.106 | −1.0 |
| O | 0.0 | 0.305 | 0.106 | −1.0 |
| Al | 0.44 | 0.152 | 0.0 | 3.0 |
| Al | 0.44 | −0.152 | 0.0 | 3.0 |
| O | 0.0 | 0.457 | 0.328 | −0.8 |
| O | 0.396 | 0.685 | 0.328 | −0.8 |
| O | 0.132 | 0.685 | 0.328 | −0.8 |
| O(OH) | 0.264 | 0.457 | 0.106 | −1.7175 |
| H(OH) | 0.35215 | 0.457 | 0.1434 | 0.7175 |
| Si | 0.0 | 0.609 | 0.273 | 1.2 |
| Si | 0.264 | 0.762 | 0.273 | 1.2 |
| O | 0.0 | 0.609 | 0.106 | −1.0 |
| O | 0.264 | 0.762 | 0.106 | −1.0 |
| Al | 0.704 | 0.609 | 0.0 | 3.0 |
| Al | 0.704 | 0.305 | 0.0 | 3.0 |
| O | 0.088 | 0.914 | −0.328 | −0.8 |
| O | 0.22 | 0.686 | −0.328 | −0.8 |
| O | −0.044 | 0.686 | −0.328 | −0.8 |
| O(OH) | 0.352 | 0.914 | −0.106 | −1.7175 |
| H(OH) | 0.26385 | 0.914 | −0.1434 | 0.7175 |
| Si | 0.088 | 0.762 | −0.273 | 1.2 |
| Si | 0.352 | 0.609 | −0.273 | 1.2 |
| O | 0.088 | 0.762 | −0.106 | −1.0 |
| O | 0.352 | 0.609 | −0.106 | −1.0 |
| O | 0.352 | 0.457 | −0.328 | −0.8 |
| O | −0.044 | 0.229 | −0.328 | −0.8 |
| O | 0.22 | 0.229 | −0.328 | −0.8 |
| O(OH) | 0.088 | 0.457 | −0.106 | −1.7175 |
| H(OH) | −0.00015 | 0.457 | −0.1434 | 0.7175 |
| Si | 0.352 | 0.305 | −0.273 | 1.2 |
| Si | 0.088 | 0.152 | −0.273 | 1.2 |
| O | 0.352 | 0.305 | −0.106 | −1.0 |
| O | 0.088 | 0.152 | −0.106 | −1.0 |

## 2. Simulation method

### 2.1. Molecular model

We use a fixed solid surface of montmorillonite clay as a 2:1 clay mineral with the unit cell formula $Na_{0.75}(Si_{7.75}Al_{0.25})(Al_{3.5}Mg_{0.5})O_{20}(OH)_4$[30]. The simulation cell contains two 32-clay unit cells resulting in a clay patch of $4.224 \times 3.656$ nm with a thickness of 0.656 nm separated by a fixed distance to represent a clay nanopore. The positions and charges of the sites in the unit cell of the clay are shown in Table 1 [37]. These positions and charges [37] have been widely used in simulations of water sorption in clay and validated by comparing to experimental data [30,38,39]. The unit cell is replicated to form the clay sheet we use in the simulations. Each of our clay sheets has 16 isomorphous replacements of trivalent Al atoms by divalent Mg atoms in the octahedral sheet, 8 isomorphous replacements of tetravalent Si atoms by trivalent Al atoms in the tetrahedral sheet, and 24 compensating monovalent sodium ions in the interlayer region [30]. In our simulation, the sheets are considered as rigid molecules; no bending potential is considered for clay sheets. The two clay sheets form a slit-like nanopore structure and sodium ions, water and gas molecules are distributed within the pore.

Methane, carbon dioxide and water molecules are simulated by using the TraPPE [40], EPM2 [41] and SPC-E [42] model,

**Table 2**
LJ parameters of methane, $CO_2$, sodium ion and atoms of clay.

| atom | $\varepsilon$ (K) | $\sigma$ (nm) | $q$ (e) |
|---|---|---|---|
| Methane | | | |
| $CH_4$ | 148.0 | 0.373 | 0 |
| Carbon dioxide | | | |
| C | 28.129 | 0.2757 | 0.6512 |
| O | 80.507 | 0.3033 | −0.3256 |
| Clay | | | |
| H | 0 | 0 | |
| O | 78.18 | 0.3166 | |
| Si | 47.803 | 0.3951 | |
| Al | 32.707 | 0.4112 | |
| Mg | 32.707 | 0.4112 | |
| Sodium ion | | | |
| $Na^+$ | 62.90 | 0.2801 | 1.0 |
| Water | | | |
| H | 0 | 0 | 0.4238 |
| O | 78.18 | 0.3166 | −0.8476 |

respectively. Sodium ions are represented by spherical particles with a point charge. Pairwise additive Lennard–Jones (LJ) and Coulomb potentials are used to compute the interactions between particles:

$$u\left(r_{ij}\right) = u^{\mathrm{LJ}} + u^{C} = 4\varepsilon_{ij}\left[\left(\frac{\sigma_{ij}}{r_{ij}}\right)^{12} - \left(\frac{\sigma_{ij}}{r_{ij}}\right)^{6}\right] + \frac{q_i q_j}{4\pi\varepsilon_0 r_{ij}}, \qquad (1)$$

in which $r_{ij}$ is the distance between sites $i$ and $j$ of different molecules, $q_i$ is the partial/full charge of the site, and $\sigma_{ij}$ and $\varepsilon_{ij}$ are LJ parameters deduced from the conventional Lorentz–Berthelot combining rules [43]. The LJ parameters of atoms of clay and sodium ions are based on the Dreiding [44,45] force-field models. Because the Dreiding force field does not include the parameter for the Mg atom, we assign Mg the same LJ parameter as Al [46]. The charges of sodium ion and Mg atom are +1e and +2e, respectively. LJ parameters and partial/full charges are listed in Table 2. All of the short-range LJ interactions are truncated at a distance of 1.07 nm. The system studied consists of the slab geometry, therefore the original three-dimensional Ewald summation is not valid. To account for periodicity in two dimensions ($x - y$ plane) and finite dimension in the third ($z$ direction), we place an empty space in the simulation cell along the $z$ direction with a length much larger than $L_x$ or $L_y$ and use the three-dimensional *Ewald* summation with correction term [47,48] to account for the long-range electrostatic interactions and the slab geometry. We allow molecules to move within the interlayer of clay sheets, but not in empty space between images of the clay sheets.

### 2.2. Simulations

The simulations for sorption of methane and $CO_2$ molecules are performed in the grand canonical ($\mu VT$) ensemble. The simulation cell is placed in a rectangular box. The box size in the $x$ direction is $L_x = 4.224$ nm, and in the $y$ direction is $L_y = 3.656$ nm. The length in the $z$ direction is determined by the pore size of the clay and the vacuum. The pore size $H$ is defined as the distance between the inner oxygen atom planes of two sheets in $z$ direction. The schematic representation of the clay nanopore is shown in Fig. 1.

The effect of water on sorption of methane and carbon dioxide is investigated in two different ways. In one, we fix the number of water molecules within the clay nanopores and simulate the sorption of methane or $CO_2$ using GCMC algorithm assuming that the pores are connected with a reservoir of pure methane or $CO_2$ with a given chemical potential $\mu$. While the number of methane or $CO_2$ molecules varies in our simulation, the number of water molecules in the pores is fixed and we allow water molecules to move in order to reach equilibrium. Similar approach

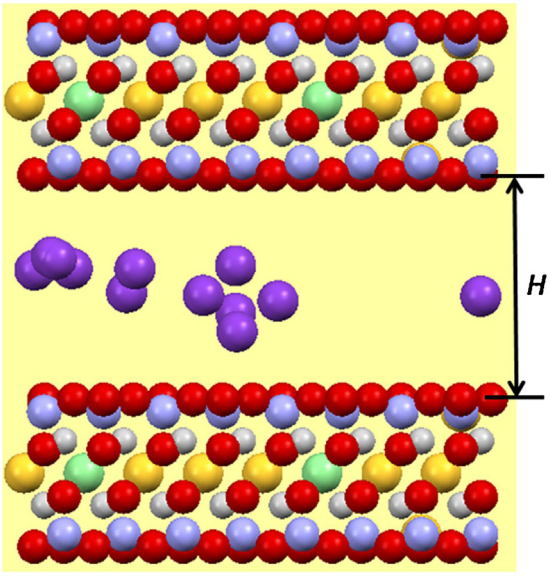


**Fig. 1.** Schematic representation of the structure of a clay nanopore. The red spheres are O atoms, the white spheres are H atoms, the yellow spheres are Si atoms, light blue spheres are Al atoms, light green spheres are Mg atoms, and purple spheres are $Na^+$ ions. (For interpretation of the references to color in this figure legend, the reader is referred to the web version of this article.)

has been used in Billemont et al. [18,19] in the study of $CO_2$ and methane sorption in presence of water in carbon nanopores. To verify whether it is reasonable to assume constant number of water molecules, the authors conducted a simple test. Starting with an initial configuration of the slit carbon nanopore filled with water, they simulated the sorption of $CO_2$ or methane at a very high fugacity. In these simulations, the amount of adsorbed water is allowed to vary as water is treated in grand canonical ensemble. No water desorption was observed even at high $CO_2$ or methane fugacities [18]. Because clay minerals are more hydrophilic than carbon materials, it is reasonable to assume that water molecules stay within the pores as gas molecules adsorb. For methane molecules, in each MC cycle, a trial random displacement is applied to all methane molecules and a methane molecule is randomly removed from or inserted into the simulation box at equal probability depending on the chemical potential of the methane reservoir outside. For simulations of $CO_2$ molecules in clay, in addition to the MC moves above, in every MC cycle, a trial random rotation is applied to all $CO_2$ molecules. We employ a biased MC algorithm to insert and remove $CO_2$ molecules [36]. For water molecules, we apply a trial random displacement and a trial random rotation in each MC cycle, and only trial random displacement move is applied to sodium ions. The chemical potentials of methane and $CO_2$ in the reservoir are obtained from the Widom insertion method [49] in canonical (NVT) ensemble without clay minerals. The MC moves are implemented by using the Metropolis algorithm [50]. The simulation consists of 0.1 million MC cycles per absorbate molecule for equilibrium and 0.5 million MC cycles per absorbate molecule for sampling the density profiles.

When the reservoir outside has a mixture of $H_2O$ and $CO_2$, with constant chemical potentials $\mu_{CO_2}$ and $\mu_{H_2O}$, we apply the GCMC algorithm to both $CO_2$ and $H_2O$ molecules within the pores and simulate the sorption of $CO_2$ and water mixtures. Within this framework, the numbers of $CO_2$ and $H_2O$ molecules within the pores are determined by the chemical potentials of $CO_2$ and $H_2O$ in the reservoir. For $CO_2$ and $H_2O$ molecules, we apply a trial random displacement, a trial random rotation and a $CO_2$ or $H_2O$ molecule is randomly removed from or inserted into the simulation box at equal probability depending on the chemical potentials of the

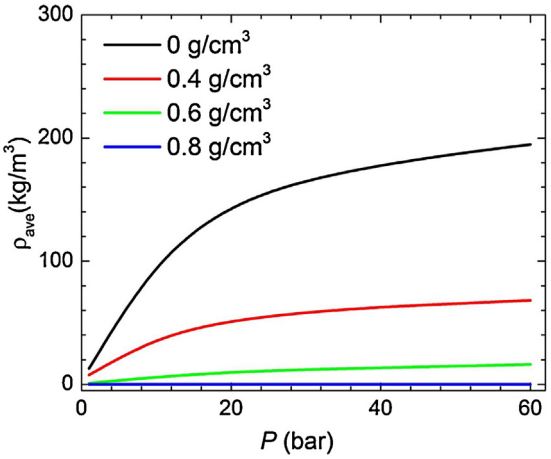


**Fig. 2.** The effect of water on sorption isotherms of methane in clay nanopores with pore size $H = 1$ nm. The black, red, green, and blue lines represent methane sorption without water, with average water density of 0.4 g/cm$^3$, with average water density of 0.6 g/cm$^3$, and with average water density of 0.8 g/cm$^3$, respectively. (For interpretation of the references to color in this figure legend, the reader is referred to the web version of this article.)

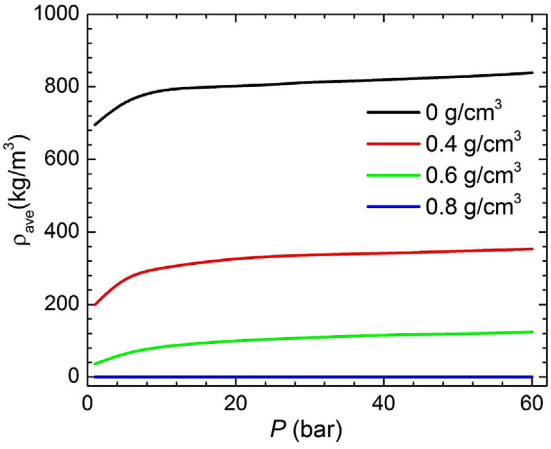


**Fig. 3.** The effect of water on sorption isotherms of $CO_2$ in clay nanopores with pore size $H = 1$ nm. The black, red, green, and blue lines represent methane sorption without water, with average water density of 0.4 g/cm$^3$, with average water density of 0.6 g/cm$^3$, and with average water density of 0.8 g/cm$^3$, respectively. (For interpretation of the references to color in this figure legend, the reader is referred to the web version of this article.)

$CO_2$ and $H_2O$ mixture in the reservoir outside. A biased MC algorithm [36] is used to insert and remove $CO_2$ or $H_2O$ molecules. The chemical potentials of $CO_2$ and $H_2O$ mixture in the reservoir are obtained from Ref. [34]. The MC moves are implemented by using the Metropolis algorithm [50]. The simulation consists of 0.1 million MC cycles per absorbate molecule for equilibrium and 0.5 million MC cycles per absorbate molecule for sampling the density profiles.

## 3. Results and discussions

### 3.1. Gas sorption with preloaded water molecules

We present the effect of water on sorption isotherm of methane and $CO_2$ in clay nanopores and density distribution for different pore sizes and pressures with varying amount of preloaded water. All of the simulations are performed at system temperature of $T = 298.15$ K.

The effect of water on sorption isotherms of methane in pore size $H = 1$ nm is presented in Fig. 2. The average gas weight density $\rho_{ave}$ in clay nanopores is given as

$$\rho_{ave} = \frac{1}{H}\int_0^H \rho(z)\,dz, \tag{2}$$

where $\rho(z)$ is the weight density at distance $z$ from one of the clay surface sheets. The average water density in the pore $\rho^{ave}_{H_2O}$ is related to the number of water molecules $N_{H_2O}$ in the pores:

$$\rho^{ave}_{H_2O} = \frac{N_{H_2O} \times M_{H_2O}}{H \times A \times N_A}, \tag{3}$$

where $A$ is the surface area of slit-pore, $N_A$ is the Avogadro number and $M_{H_2O}$ is the water molar weight.

As seen in Fig. 2 in pore size $H = 1$ nm, methane sorption decreases significantly as the average water density increases. Water molecule has a strong dipole moment, while methane is charge neutral. In a previous work [14], we have shown that methane sorption in dry clay nanopores is dominated by surface adsorption. Water molecules have strong affinity to clay surface atoms reducing methane adsorption. At a water content corresponding to $\rho^{ave}_{H_2O} = 0.4$ g/cm$^3$, methane sorption reduces 3 times at a high pressure ($P = 60$ bar). At a high water content corresponding to $\rho^{ave}_{H_2O} = 0.8$ g/cm$^3$, methane sorption in nanopores becomes negligible. In a small pore, as pressure increases, methane sorption reaches a plateau in both dry and wet clay pores. As we will see later, methane molecules are adsorbed in the same layer as water due to the wall interactions from the two sides.

The effect of water on sorption isotherms of $CO_2$ in clay nanopores in pore size $H = 1$ nm is presented in Fig. 3. Similar to methane sorption, water substantially reduces $CO_2$ sorption. In a dry condition, due to the cation exchange, $CO_2$ sorption capacity is high [14]. However, as more water molecules are attracted to the clay surface, the contribution from $CO_2$ surface adsorption is greatly reduced. Although $CO_2$ has a quadruple moment, the dipole moment of water molecule makes it having stronger affinity than $CO_2$ to the clay surface. With water, because water molecules are strongly adsorbed onto the clay surfaces, $CO_2$ adsorption layer is substantially reduced as we show later. Charged atoms on the clay surfaces significantly increase $CO_2$ sorption and surface adsorption is the main contribution in a dry clay nanopore [14]. As a result, in small pores (1 nm), reduction in $CO_2$ sorption in clay nanopore is more significant than that of methane. In contrast to clay minerals, the reduction in methane sorption is greater than that of $CO_2$ in presence of water in carbon nanopores [18]. This is probably because there are no charged atoms on carbon surface [18] and $CO_2$ sorption is less pronounced. A significant difference between Figs. 2 and 3 is the pronounced sorption of $CO_2$ at low pressure at all conditions, which is mainly because the cation exchange of montmorillonite provides additional charged molecules (sodium ions) to greatly enhance $CO_2$–clay interaction.

Fig. 4 presents the effect of water on sorption isotherms of methane in clay nanopores in pore size $H = 4$ nm. Note that the effect of pressure is very different in Figs. 2 and 4. But similar to a small pore ($H = 1$ nm), water greatly reduces methane sorption. In contrast to Fig. 2, methane sorption increases with bulk pressures in both dry and wet nanopores because in large pores, methane molecules can accumulate in the middle of the pores. However, at high water content ($\rho^{ave}_{H_2O} = 0.8$ g/cm$^3$), the increase in sorption with pressure is small because water not only adsorbs on surfaces but also occupies the space in the middle of pores. The effect of water on sorption isotherms of $CO_2$ in clay nanopores in a pore of size $H = 4$ nm is presented in Fig. 5. This plot shows that the sorption cannot be described by Langmuir isotherm for

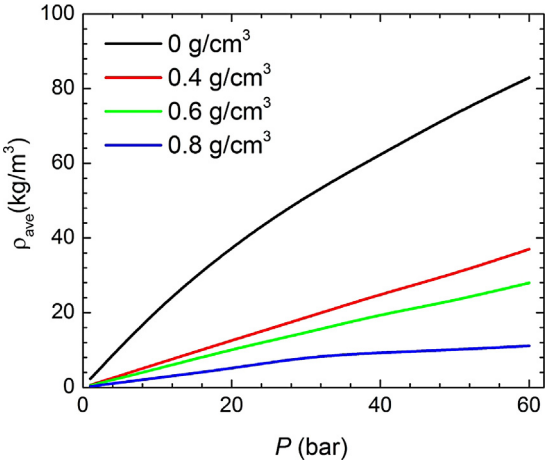


**Fig. 4.** The same as Fig. 2, but for $H = 4$ nm.

dry and low density water preload condition. In dry condition, due to strong $CO_2$–surface interaction, $CO_2$ may have a multi-layer adsorption and sorption increases with pressure. In general, water reduces $CO_2$ sorption. However, when $P \leq 40$ bar, sorption is comparable for $\rho^{ave}_{H_2O} = 0.4$ g/cm$^3$ and $\rho^{ave}_{H_2O} = 0.6$ g/cm$^3$ and slightly higher sorption is observed at $\rho^{ave}_{H_2O} = 0.6$ g/cm$^3$. The presence of water results in gas mainly in the middle of the pores. With moderate water amount, the effect of water on the gas in the middle of the pores is not significant at low pressure. As pressure increases, $CO_2$ sorption is higher with less water. At low water content ($\rho^{ave}_{H_2O} = 0.4$ g/cm$^3$), $CO_2$ sorption gradually increases with pressure, because with small amount of water, $CO_2$ still can have a multi-layer adsorption. At high water content ($\rho^{ave}_{H_2O} = 0.8$ g/cm$^3$), $CO_2$ sorption is greatly reduced and quickly reaches a plateau as pressure increases. Large amount of water in the middle of the pores hampers $CO_2$ sorption.

To better understand the effect of water on the structural behavior of gas sorption, we present the weight density distributions of methane molecules at bulk pressure $P = 40$ bar in different pore sizes in Fig. 6. In small pores ($H = 1$ nm), methane molecules adsorb onto the clay surface regardless of the water content, but the strength of adsorption layer decreases as water increases. As the pore size increases, methane molecules do not adsorb onto the same layer as water molecules but they form a second adsorbed layer (Fig. 6b). Methane molecules can also be seen in the middle of the pores. In all pore sizes, water molecules are adsorbed onto

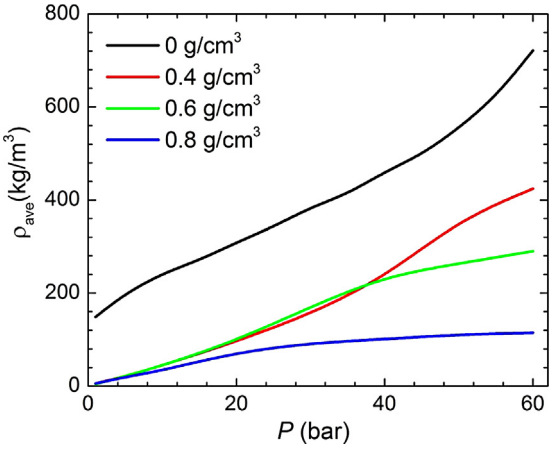


**Fig. 5.** The same as Fig. 4, but for $CO_2$.

the clay surfaces due to the charge of clay atoms. Because of weak short-range methane–clay interactions, methane forms a weak adsorption layer next to water adsorption layer. In larger pores ($H \geq 3$ nm), for moderate water densities ($\rho^{ave}_{H_2O} = 0.4$ g/cm$^3$ and $\rho^{ave}_{H_2O} = 0.6$ g/cm$^3$), the methane density distribution in the middle of the pore slightly exceeds the bulk limit. In the middle of the pores, water and methane may form a certain structure due to water–methane interactions. Previous works have shown that methane sorption in clay minerals are mainly due to surface adsorption [7,14]. Water molecules form a strong adsorption layer preventing the formation of methane adsorption layer onto the surface. As a result, methane sorption is greatly reduced in clay nanopores.

The effect of water on weight density distributions of $CO_2$ molecules at bulk pressure $P = 40$ bar in different pore sizes is presented in Fig. 7. In general, $CO_2$ density profile is similar to methane but the adsorption layer is stronger. In small pores ($H = 1$ nm), $CO_2$ molecules are adsorbed onto the clay surface. But because water molecules predominantly adsorb on the surface, $CO_2$ sorption is greatly reduced. In larger pores ($H \geq 2$ nm), $CO_2$ molecules are not seen in the first adsorbed layer; they form a second weak adsorption layer. $CO_2$ molecules also accumulate in the middle of the pores. For small amount of water ($\rho^{ave}_{H_2O} = 0.4$ g/cm$^3$), due to the strong $CO_2$–$H_2O$ interactions, $CO_2$ density distribution in the middle of the pores is higher than that without water. Comparing to methane, the electrostatic interaction between $CO_2$ and $H_2O$ is strong and can partially compensate the loss of $CO_2$ sorption due to water. However, if water density is high ($\rho^{ave}_{H_2O} = 0.8$ g/cm$^3$), because water would essentially fill up the pores, the $CO_2$ molecules in the middle of the pores becomes less significant.

The weight density distributions of $H_2O$ molecules at bulk pressure $P = 40$ bar are shown in Fig. 8 for the system of Fig. 7. Note that in all the plots the location of the main adsorbed layer stays the same irrespective of water content. In small pores ($H = 1$ nm), water molecules are adsorbed onto the clay surfaces because of the charges of clay atoms. As a result, $CO_2$ adsorption layer is greatly diminished. As pore size increases, water molecules are first adsorbed onto the clay surfaces and once the adsorption layer is packed, they fill the middle of the pores. For moderate water content ($\rho^{ave}_{H_2O} = 0.4$ g/cm$^3$ and $\rho^{ave}_{H_2O} = 0.6$ g/cm$^3$), the accumulation of water molecules in the middle of the pores are not strong, thus $CO_2$ molecules can fill the space. However, when the water content is high ($\rho^{ave}_{H_2O} = 0.8$ g/cm$^3$), water molecules fill the middle of the pores and as a result, $CO_2$ content is greatly reduced. In larger pores ($H \geq 2$ nm), because water molecules dominate the surface adsorption layer, adsorption layer of $CO_2$ on the clay surfaces is not observed.

Next we study the effect of water on weight density distribution of methane at high pressure of $P = 100$ bar in different pore sizes presented in Fig. 9. In small pores ($H = 1$ nm), the methane density distributions resemble that at the lower pressure of $P = 40$ bar. The density distribution of the adsorbed layer is higher than the larger pores due to the effect of the two walls. As pore size increases, methane molecules start to accumulate in the middle of the pores. In $H = 2$ nm, at water average density of $\rho^{ave}_{H_2O} = 0.4$ g/cm$^3$, the first peak of methane density distribution is higher than the second peak of methane density distribution in the dry condition due to the methane–$H_2O$ interactions. However, as water average density increases, the first peak in methane density distribution is lower than the second peak of pure methane. In larger pores ($H \geq 3$ nm), the methane density distribution in the middle of pores approaches bulk limit except for water average density of $\rho^{ave}_{H_2O} = 0.8$ g/cm$^3$. The weight density distributions of $CO_2$ molecules at bulk pressure $P = 100$ bar in different size pores are presented in Fig. 10. In this condition, $CO_2$ is in liquid state. In dry condition, $CO_2$ forms

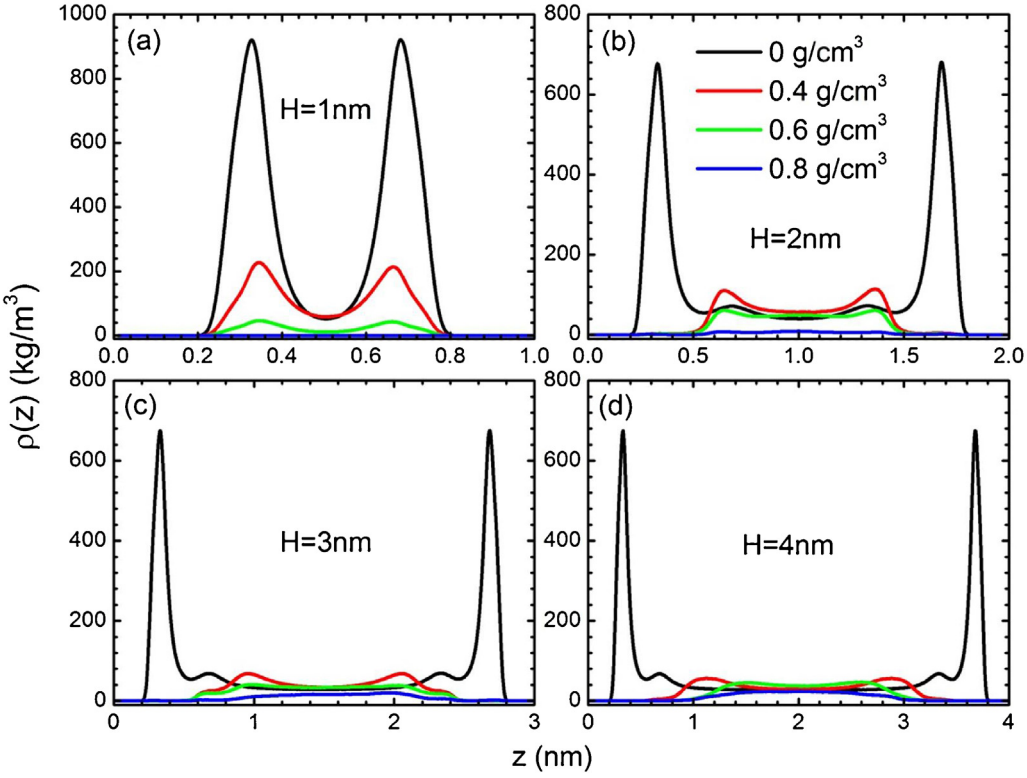


**Fig. 6.** The weight density distributions of methane molecules at bulk pressure $P = 40$ bar and temperature $T = 298.15$ K in clay nanopores with pore size (a) $H = 1$ nm. (b) $H = 2$ nm. (c) $H = 3$ nm. (d) $H = 4$ nm. The black, red, green, and blue lines represent the methane density distribution at dry condition, with average water density of 0.4 g/cm$^3$, with average water density of 0.6 g/cm$^3$, and with average water density of 0.8 g/cm$^3$, respectively.

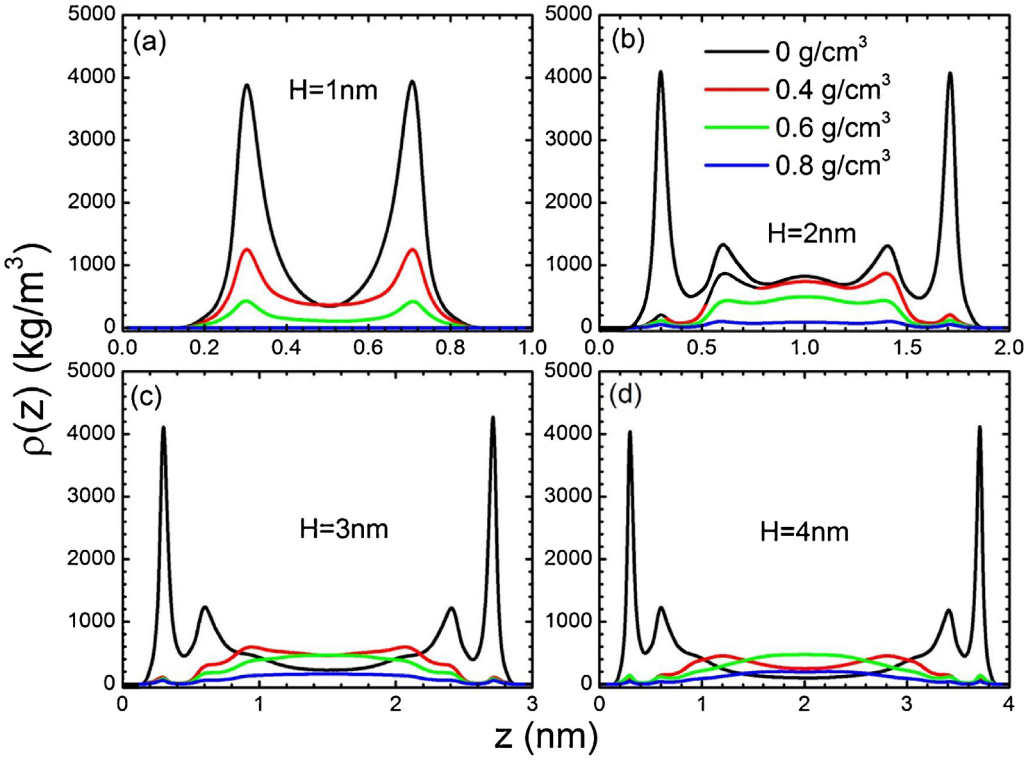


**Fig. 7.** The same as Fig. 6, but for $CO_2$ molecules.

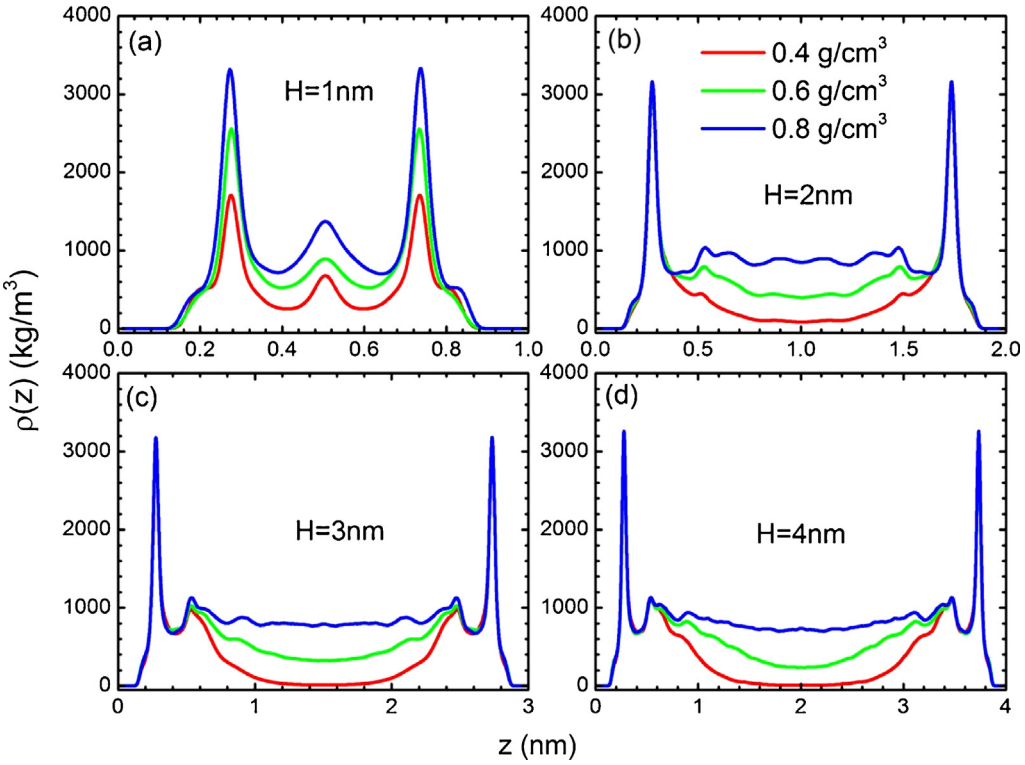


**Fig. 8.** The weight density distributions of water molecules in the $CO_2$–preloaded water system at $CO_2$ bulk pressure $P = 40$ bar and temperature $T = 298.15$ K in clay nanopores with pore size (a) $H = 1$ nm. (b) $H = 2$ nm. (c) $H = 3$ nm. (d) $H = 4$ nm. The red, green, and blue lines represent the water density distribution with average water density of 0.4 g/cm$^3$, 0.6 g/cm$^3$, and 0.8 g/cm$^3$, respectively. (For interpretation of the references to color in this figure legend, the reader is referred to the web version of this article.)

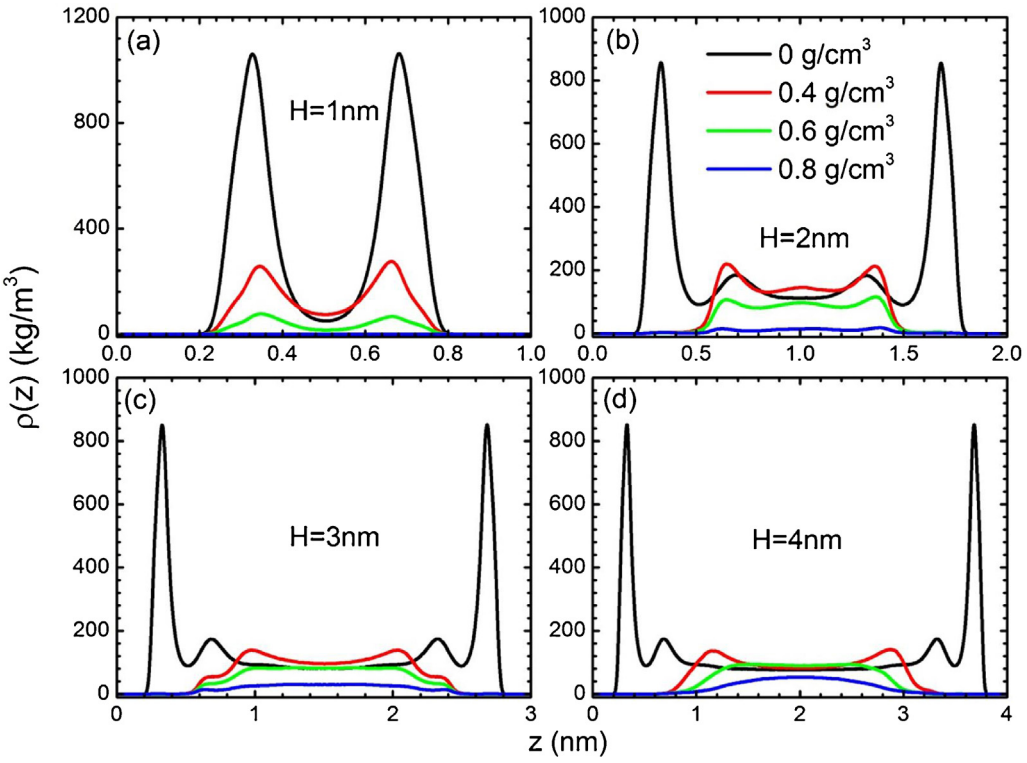


**Fig. 9.** The weight density distributions of methane molecules at bulk pressure $P = 100$ bar and temperature $T = 298.15$ K in clay nanopores with pore size (a) $H = 1$ nm. (b) $H = 2$ nm. (c) $H = 3$ nm. (d) $H = 4$ nm. The black, red, green, and blue lines represent the methane density distribution at dry condition, and average water density of 0.4 g/cm$^3$, 0.6 g/cm$^3$, and 0.8 g/cm$^3$, respectively. (For interpretation of the references to color in this figure legend, the reader is referred to the web version of this article.)

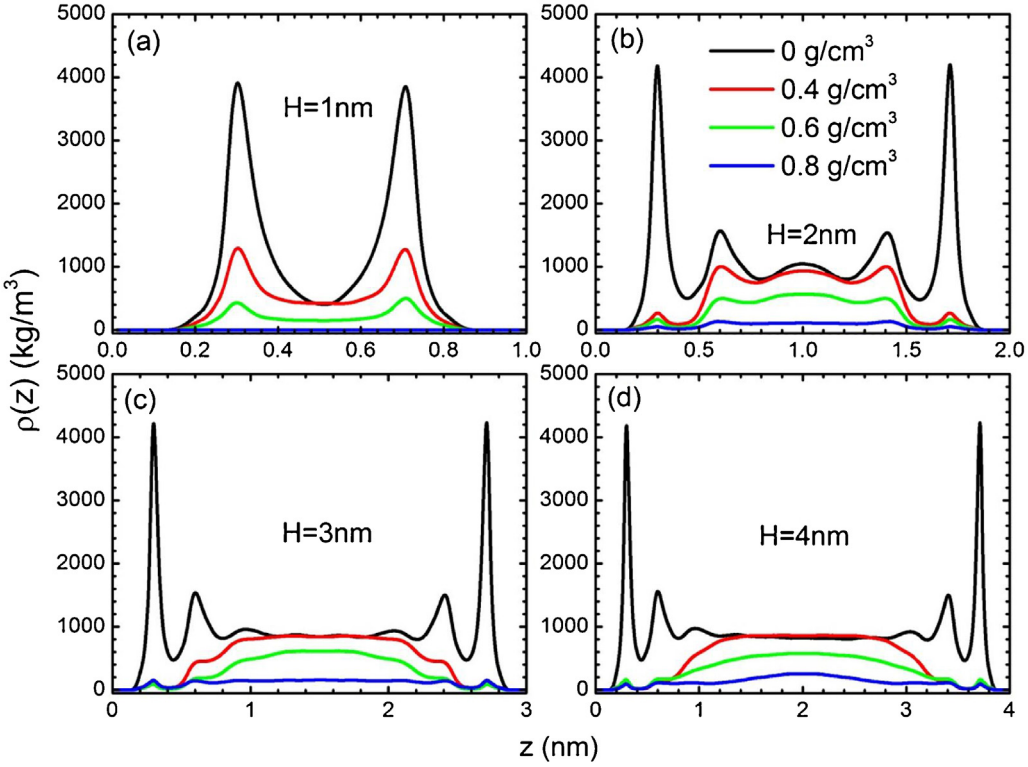


**Fig. 10.** The same as Fig. 9, but for $CO_2$ molecules.

multi-layer adsorption. But in the presence of water, because water reduces accessible pore volume of $CO_2$, in all pore sizes, $CO_2$ sorption is greatly reduced. Thus, only when water average density is low ($\rho^{ave}_{H_2O} = 0.4$ g/cm$^3$), the $CO_2$ density distribution in the middle of the pores reaches bulk limit in large pores. As water density increases, the density of liquid phase $CO_2$ in the pores decreases.

The snapshots of MC simulations for configurations of methane and $CO_2$ molecules in the pores corresponding to Figs. 9 and 10 can be seen in Figs. 11 and 12, respectively. For methane molecules as depicted in Fig. 11, in a small pore ($H = 1$ nm) with low water density ($\rho^{ave}_{H_2O} = 0.4$ g/cm$^3$), water molecules are adsorbed onto the clay surface because of the negatively charged clay sheets. Methane molecules are also adsorbed to the clay surface due to correlations between the two walls and small pore spaces. In larger pores ($H = 4$ nm) with the same water density, water molecules are adsorbed on the clay surface, while methane molecules can only be seen in the middle of the pores. Beyond the water adsorption layer, we observe methane adsorption layer due to water–methane interactions. In a small pore ($H = 1$ nm) with high water density ($\rho^{ave}_{H_2O} = 0.8$ g/cm$^3$), because water molecules essentially fill up the pore, there is no space for methane molecules. In larger pores ($H = 4$ nm) with the same water density, water molecules cover the clay surfaces and greatly reduce the accessible pore volume for methane molecules. As a result, only a small number of methane molecules are observed in middle of the pore. Because methane is hydrophobic, methane molecules do not spread within water molecules but accumulate together.

In the preloaded water for the water–$CO_2$ systems, in a small pore ($H = 1$ nm) with low water density ($\rho^{ave}_{H_2O} = 0.4$ g/cm$^3$), Fig. 12 shows that both water and $CO_2$ molecules are adsorbed onto the clay surfaces, while water molecules dominate the adsorption layer. In larger pores ($H = 4$ nm) with the same water density, water molecules are adsorbed onto the clay surfaces while $CO_2$ molecules are in the middle of the pore. In a small pore ($H = 1$ nm) with high water density ($\rho^{ave}_{H_2O} = 0.8$ g/cm$^3$), water molecules occupy the pore and there is no room for $CO_2$ molecules. In larger pores ($H = 4$ nm) with the same water density, $CO_2$ molecules are observed in the middle of the pore. Similar to methane molecules, $CO_2$ molecules accumulate together.

### 3.2. $CO_2$ sorption from mixtures of $CO_2$ and $H_2O$ in the reservoir

We present the density distribution of water and $CO_2$ molecules in different pore sizes by fixing composition in the exterior reservoir. The computations are based on the chemical potentials in a $CO_2$-rich phase with $CO_2$ mole fraction $x_{CO_2} = 0.994$ in the exterior reservoir from Ref. [34]. All of the simulations are performed at temperature of $T = 348.15$ K.

The weight density distributions of $CO_2$ and water molecules in the nanopores at bulk pressure $P = 125$ bar in different pore sizes are presented in Fig. 13. For comparison, we also show the density distribution of pure $CO_2$ molecules at the same pressure and temperature. In the small pore ($H = 1$ nm), even though the water content in reservoir outside is less than 1%, the water adsorption layer dominates and there is a weak $CO_2$ adsorption layer. The position of the peak $CO_2$ density distribution of the water and $CO_2$ mixture is the same as pure $CO_2$, but $CO_2$ adsorption is greatly diminished. As the pore size increases, water molecules are mainly adsorbed onto the clay surfaces and a weak $CO_2$ adsorption layer forms close to surface. Because water molecules are only adsorbed on the surface, $CO_2$ forms an adsorption layer next to the water adsorption layer and $CO_2$ in the middle of the pores resembles that of pure $CO_2$. As a result, the second peak in $CO_2$ density distribution is stronger than the first peak. Due to strong water–clay interactions, water molecules mainly adsorbed onto the clay surfaces resulting in much less $CO_2$ sorption. On the other hand, $CO_2$ sorption in clay nanopores in a dry condition is mainly due to surface adsorption [14]. Overall, even with little amount of water in the

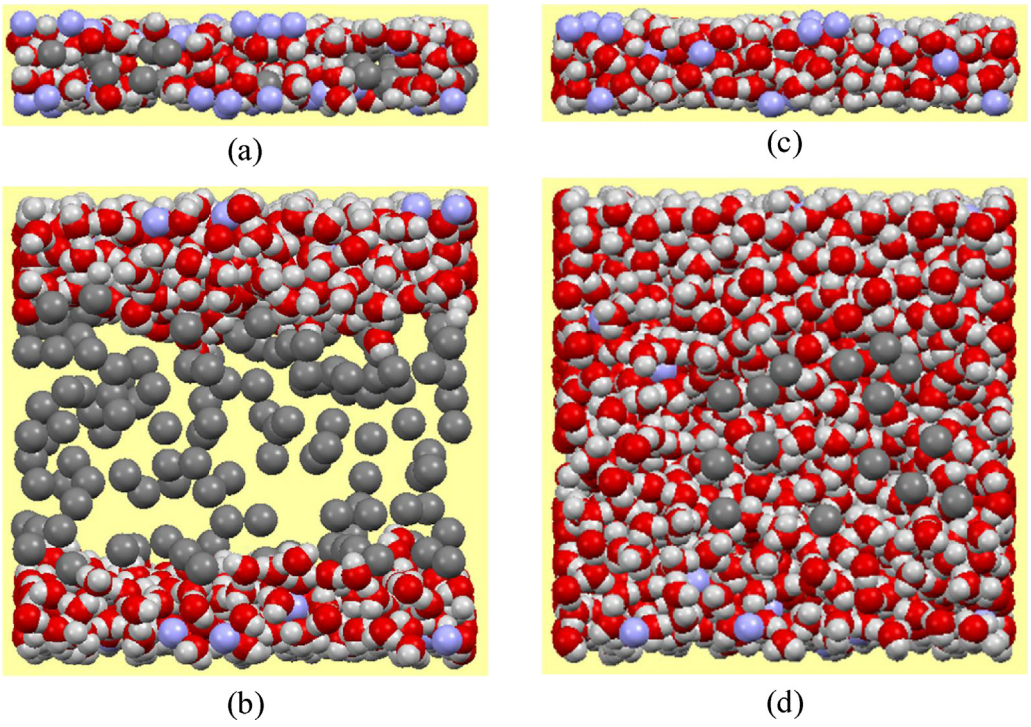


**Fig. 11.** The snapshot of methane and water molecules for methane pressure $P = 100$ bar in a clay nanopore of (a) $H = 1$ nm and average water density of 0.4 g/cm$^3$. (b) $H = 4$ nm and average water density of 0.4 g/cm$^3$. (c) $H = 1$ nm and average water density of 0.8 g/cm$^3$. (d) $H = 4$ nm and average water density of 0.8 g/cm$^3$. The gray spheres are $C_1$, the red and light gray spheres are O and H atoms of water molecules, respectively, and light blue spheres are $Na^+$. In all of figures, the structure of clay is omitted. (For interpretation of the references to color in this figure legend, the reader is referred to the web version of this article.)

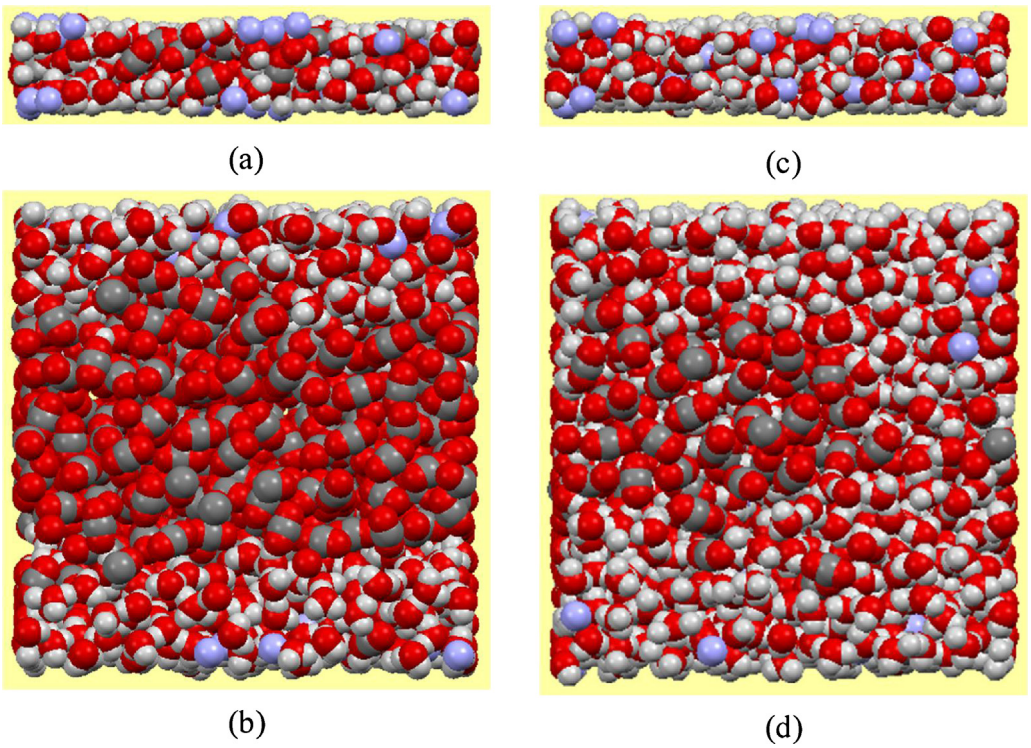


**Fig. 12.** The snapshot of $CO_2$ and water molecules at $CO_2$ pressure $P = 100$ bar in a clay nanopore of (a) $H = 1$ nm and average water density of 0.4 g/cm$^3$. (b) $H = 4$ nm and average water density of 0.4 g/cm$^3$. (c) $H = 1$ nm and average water density of 0.8 g/cm$^3$. (d) $H = 4$ nm and average water density of 0.8 g/cm$^3$. The gray spheres are C atoms of $CO_2$ molecule, the red spheres are O atoms of water and $CO_2$ molecules, the light gray spheres are H atoms of water molecules, and light blue spheres are $Na^+$. In all of figures, the structure of clay is omitted. (For interpretation of the references to color in this figure legend, the reader is referred to the web version of this article.)

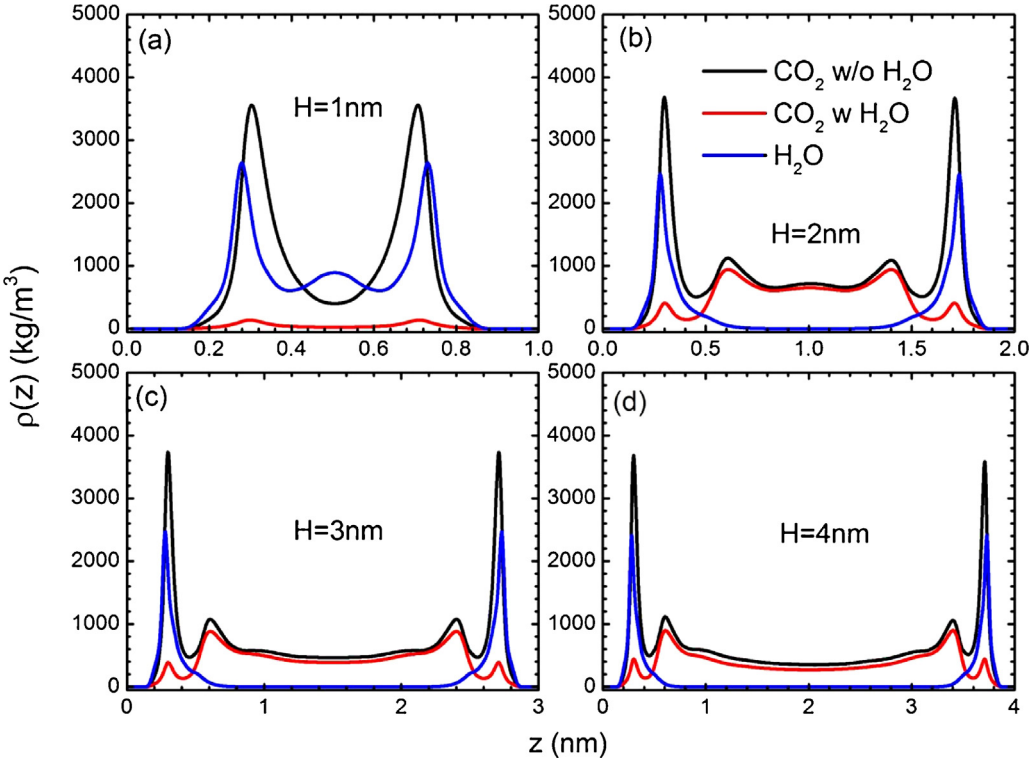


**Fig. 13.** The weight density distributions of $CO_2$ and water molecules for reservoir of $CO_2$ mole fraction $x_{CO_2} = 0.994$ at bulk pressure $P = 125$ bar and temperature $T = 348.15$ K in clay nanopores of (a) $H = 1$ nm. (b) $H = 2$ nm. (c) $H = 3$ nm. (d) $H = 4$ nm. The black, red, and blue lines represent the pure $CO_2$ density distribution at the same pressure and temperature without water, the $CO_2$ density distribution of $CO_2$–water mixtures, and the water density distribution of $CO_2$–water mixtures, respectively. (For interpretation of the references to color in this figure legend, the reader is referred to the web version of this article.)

reservoir outside the nanopore, $CO_2$ sorption in clay minerals are significantly reduced.

## 4. Conclusions

Our investigation reveals that methane and $CO_2$ sorption in clay nanopores are greatly reduced by water. This is because water molecules cover the clay surfaces forming water adsorption layer due to the hydrophilic clay surfaces. In a previous study we have shown that surface adsorption is stronger in $CO_2$ than methane in dry conditions [14]. Water has a significant effect on adsorption of $CO_2$ and methane. When the pore size is 1 nm, water and $CO_2$, and water and methane adsorb in the same layer. In pores larger than 1 nm, that is, in pores of 2, 3, and 4 nm, water adsorbs onto the first layer, and $CO_2$ and methane form a second weaker layer next the water adsorbed layer. The $CO_2$ adsorbed layer is stronger than the methane adsorbed layer. $CO_2$ and methane molecules also accumulate in the middle of larger pores as pressure increases.

Water greatly reduces the $CO_2$ sorption in clay nanopores, even at very low water concentration in the exterior reservoir (mole fraction less than 0.01). We observe a strong water adsorption layer but a weak $CO_2$ adsorption layer onto the clay surfaces. As the pore size increases, a second peak in $CO_2$ density distribution forms due to $CO_2$–water interactions and $CO_2$ molecules accumulate in the middle of pores.

We also observe the formation of a strong second adsorbed layer of $CO_2$ both in pure dry and low water content conditions. The second layer becomes stronger with increasing pressure. As a result of the second layer, Langmuir adsorption model cannot describe $CO_2$ sorption.

## Acknowledgement

This work was supported by member companies of the Reservoir Engineering Research Institute. Their support is greatly appreciated.

## References

[1] T. Zhang, G.S. Ellis, S.C. Ruppel, K. Milliken, R. Yang, Effect of organic-matter type and thermal maturity on methane adsorption in shale-gas systems, Org. Geochem. 47 (2012) 120–131.
[2] C.H. Sondergeld, R.J. Ambrose, C.S. Rai, J. Moncrieff, Micro-structural Studies of Gas Shales, Society of Petroleum Engineers, Pittsburgh, Pennsylvania, 2010, pp. 131771.
[3] D.J.K. Ross, R. Marc Bustin, The importance of shale composition and pore structure upon gas storage potential of shale gas reservoirs, Mar. Pet. Geol. 26 (2009) 916–927.
[4] D.J.K. Ross, R.M. Bustin, Characterizing the shale gas resource potential of Devonian–Mississippian strata in the Western Canada sedimentary basin: application of an integrated formation evaluation, AAPG Bull. 92 (2008) 87–125.
[5] P. Weniger, W. Kalkreuth, A. Busch, B.M. Krooss, High-pressure methane and carbon dioxide sorption on coal and shale samples from the Paraná Basin, Brazil, Int. J. Coal Geol. 84 (2010) 190–205.
[6] M. Gasparik, P. Bertier, Y. Gensterblum, A. Ghanizadeh, B.M. Krooss, R. Littke, Geological controls on the methane storage capacity in organic-rich shales, Int. J. Coal Geol. 123 (2014) 34–51.
[7] L. Ji, T. Zhang, K.L. Milliken, J. Qu, X. Zhang, Experimental investigation of main controls to methane adsorption in clay-rich rocks, Appl. Geochem. 27 (2012) 2533–2545.
[8] R. Aringhieri, Nanoporosity characteristics of some natural clay minerals and soils, Clays Clay Miner. 52 (2004) 700–704.
[9] C.-C. Wang, L.-C. Juang, C.-K. Lee, T.-C. Hsu, J.-F. Lee, H.-P. Chao, Effects of exchanged surfactant cations on the pore structure and adsorption characteristics of montmorillonite, J. Colloid Interface Sci. 280 (2004) 27–35.
[10] P.D. Schettler Jr., C.R. Parmely, Contributions to total storage capacity in devonian shales, in: SPE, J, SPE 23422, 1991.
[11] X.-C. Lu, F.-C. Li, A.T. Watson, Adsorption studies of natural gas storage in devonian shales, in: SPE Formation Evaluation, SPE 26632, 1995.

[12] A. Busch, S. Alles, Y. Gensterblum, D. Prinz, D.N. Dewhurst, M.D. Raven, H. Stanjek, B.M. Krooss, Carbon dioxide storage potential of shales, Int. J. Greenhouse Gas Control 2 (2008) 297–308.
[13] M. Gasparik, A. Ghanizadeh, P. Bertier, Y. Gensterblum, S. Bouw, B.M. Krooss, High-pressure methane sorption isotherms of black shales from The Netherlands, Energy Fuels 26 (2012) 4995–5004.
[14] Z. Jin, A. Firoozabadi, Methane and carbon dioxide adsorption in clay-like slit pores by Monte Carlo simulations, Fluid Phase Equilib. 360 (2013) 456–465.
[15] V. Marry, P. Turq, T. Cartailler, D. Levesque, Microscopic simulation of structure and dynamics of water and counterions in a monohydrated montmorillonite, J. Chem. Phys. 117 (2002) 3454–3463.
[16] C.D. Jenkins, Coalbed- and shale-gas reservoirs, J. Pet. Technol. 60 (2008) 92–99.
[17] M. Gasparik, A. Ghanizadeh, Y. Gensterblum, B.M. Krooss, R. Littke, The methane storage capacity of black shales, in: 3rd EAGE Shale Wrokshop, 2012.
[18] P. Billemont, B. Coasne, G. De Weireld, An experimental and molecular simulation study of the adsorption of carbon dioxide and methane in nanoporous carbons in the presence of water, Langmuir 27 (2010) 1015–1024.
[19] P. Billemont, B. Coasne, G. De Weireld, Adsorption of carbon dioxide, methane, and their mixtures in porous carbons: effect of surface chemistry, water content, and pore disorder, Langmuir 29 (2013) 3328–3338.
[20] A. Busch, Y. Gensterblum, B.M. Krooss, Methane and $CO_2$ sorption and desorption measurements on dry Argonne premium coals: pure components and mixtures, Int. J. Coal Geol. 55 (2003) 205–224.
[21] S. Ottiger, R. Pini, G. Storti, M. Mazzotti, Measuring and modeling the competitive adsorption of $CO_2$, $CH_4$, and $N_2$ on a dry coal, Langmuir 24 (2008) 9531–9540.
[22] S. Ottiger, R. Pini, G. Storti, M. Mazzotti, Competitive adsorption equilibria of $CO_2$ and $CH_4$ on a dry coal, Adsorption 14 (2008) 539–556.
[23] S.A. Mohammad, K.A.M. Gasem, Modeling the competitive adsorption of $CO_2$ and water at high pressures on wet coals, Energy Fuels 26 (2011) 557–568.
[24] S. Day, R. Sakurovs, S. Weir, Supercritical gas sorption on moist coals, Int. J. Coal Geol. 74 (2008) 203–214.
[25] Y. Sun, Y. Wang, Y. Zhang, Y. Zhou, L. Zhou, $CO_2$ sorption in activated carbon in the presence of water, Chem. Phys. Lett. 437 (2007) 14–16.
[26] Y. Sun, Q. Xue, Y. Zhou, L. Zhou, Sorption equilibria of $CO_2/CH_4$ mixture on activated carbon in presence of water, J. Colloid Interface Sci. 322 (2008) 22–26.
[27] M. Švábová, Z. Weishauptová, O. Přibyl, The effect of moisture on the sorption process of $CO_2$ on coal, Fuel 92 (2012) 187–196.
[28] Y. Wang, Y. Zhou, C. Liu, L. Zhou, Comparative studies of $CO_2$ and $CH_4$ sorption on activated carbon in presence of water, Colloids Surf., A: Physicochem. Eng. Aspects 322 (2008) 14–18.
[29] A. Hildenbrand, B.M. Krooss, A. Busch, R. Gaschnitz, Evolution of methane sorption capacity of coal seams as a function of burial history—a case study from the Campine Basin, NE Belgium, Int. J. Coal Geol. 66 (2006) 179–203.
[30] M. Chavez-Paez, K.V. Workum, L.d. Pablo, J.J.d. Pablo, Monte Carlo simulations of Wyoming sodium montmorillonite hydrates, J. Chem. Phys. 114 (2001) 1405–1413.
[31] R.T. Cygan, V.N. Romanov, E.M. Myshakin, Molecular simulation of carbon dioxide capture by montmorillonite using an accurate and flexible force field, J. Phys. Chem. C 116 (2012) 13079–13091.
[32] X. Yang, C. Zhang, Structure and diffusion behavior of dense carbon dioxide fluid in clay-like slit pores by molecular dynamics simulation, Chem. Phys. Lett. 407 (2005) 427–432.
[33] J. Zhang, M.B. Clennell, D. Dewhurst, K. Liu, Combined Monte Carlo and molecular dynamics simulation of methane adsorption on dry and moist coal, Fuel 122 (2014) 186–197.
[34] A. Botan, B. Rotenberg, V. Marry, P. Turq, B. Noetinger, Carbon dioxide in montmorillonite clay hydrates: thermodynamics, structure, and transport from molecular simulation, J. Phys. Chem. C 114 (2010) 14962–14969.
[35] G. Sposito, N.T. Skipper, R. Sutton, S.-h. Park, A.K. Soper, J.A. Greathouse, Surface geochemistry of the clay minerals, Proc. Nat. Acad. Sci. U.S.A. 96 (1999) 3358–3364.
[36] E.J.M. Hensen, T.J. Tambach, A. Bliek, B. Smit, Adsorption isotherms of water in Li-, Na-, and K-montmorillonite by molecular simulation, J. Chem. Phys. 115 (2001) 3322–3329.
[37] N.T. Skipper, F.-R. Chou Chang, G. Sposito, Monte Carlo simulation of interlayer molecular structure in swelling clay minerals. 1. Methodology, Clays Clay Miner. 43 (1995) 285–293.
[38] F.-R.C. Chang, N.T. Skipper, G. Sposito, Monte Carlo and molecular dynamics simulations of interfacial structure in lithium-montmorillonite hydrates, Langmuir 13 (1997) 2074–2082.
[39] F.-R.C. Chang, N.T. Skipper, G. Sposito, Computer simulation of interlayer molecular structure in sodium montmorillonite hydrates, Langmuir 11 (1995) 2734–2741.
[40] M.G. Martin, J.I. Siepmann, Transferable potentials for phase equilibria. 1. United-atom description of *n*-alkanes, J. Phys. Chem. B 102 (1998) 2569–2577.
[41] J.G. Harris, K.H. Yung, Carbon Dioxide's liquid–vapor coexistence curve and critical properties as predicted by a simple molecular model, J. Phys. Chem. 99 (1995) 12021–12024.
[42] H.J.C. Berendsen, J.R. Grigera, T.P. Straatsma, The missing term in effective pair potentials, J. Phys. Chem. 91 (1987) 6269–6271.
[43] D. Frankel, B. Smit, Understanding Molecular Simulation: From Algorithms to Applications, Academic Press, London, 2002.
[44] K.S. Smirnov, D. Bougeard, A molecular dynamics study of structure and short-time dynamics of water in kaolinite, J. Phys. Chem. B 103 (1999) 5266–5273.
[45] S.L. Mayo, B.D. Olafson, W.A. Goddard, DREIDING: a generic force field for molecular simulations, J. Phys. Chem. 94 (1990) 8897–8909.
[46] Q.H. Zeng, A.B. Yu, G.Q. Lu, R.K. Standish, Molecular dynamics simulation of organic–inorganic nanocomposites: layering behavior and interlayer structure of organoclays, Chem. Mater. 15 (2003) 4732–4738.
[47] I.-C. Yeh, M.L. Berkowitz, Ewald summation for systems with slab geometry, J. Chem. Phys. 111 (1999) 3155–3162.
[48] P.S. Crozier, R.L. Rowley, E. Spohr, D. Henderson, Comparison of charged sheets and corrected 3D Ewald calculations of long-range forces in slab geometry electrolyte systems with solvent molecules, J. Chem. Phys. 112 (2000) 9253–9257.
[49] B. Widom, Some topics in the theory of fluids, J. Chem. Phys. 39 (1963) 2808–2812.
[50] N. Metropolis, A.W. Rosenbluth, M.N. Rosenbluth, A.H. Teller, E. Teller, Equation of state calculations by fast computing machines, J. Chem. Phys. 21 (1953) 1087–1092.